

Spin effects in electron tunnelling through a quantum dot coupled to non-collinearly polarized ferromagnetic leads

W. Rudziński¹, J. Barnasć^{1,2}, R. Świrkowicz³, and M. Wilczyński³

¹Department of Physics, Adam Mickiewicz University, ul. Umultowska 85, 61-614 Poznań, Poland

²Institute of Molecular Physics, Polish Academy of Sciences,
ul. Smoluchowskiego 17, 60-179 Poznań, Poland

³Faculty of Physics, Warsaw University of Technology, ul. Koszykowa 75, 00-662 Warszawa, Poland

(Dated: November 1, 2018)

Spin-dependent transport through an interacting single-level quantum dot coupled to ferromagnetic leads with non-collinear magnetizations is analyzed theoretically. The transport properties and average spin of the dot are investigated within the nonequilibrium Green function technique based on the equation of motion in the Hartree-Fock approximation. Numerical results show that Coulomb correlations on the dot and strong spin polarization of the leads significantly enhance precession of the average dot spin around the effective molecular field created by the external electrodes. Moreover, they also show that spin precession may lead to negative differential conductance in the voltage range between the two relevant threshold voltages. Nonmonotonous angular variation of electric current and change in sign of the tunnel magnetoresistance are also found. It is also shown that the diode-like behavior in asymmetrical junctions with one electrode being half-metallic is significantly reduced in noncollinear configurations.

PACS numbers: 72.25.Mk; 73.63.Kv; 73.23.Hk

I. INTRODUCTION

Current interest in electronic transport and spin effects in mesoscopic tunnel junctions is stimulated by their possible applications in microelectronics and spintronics devices [1, 2]. One of the most widely studied spin-dependent effects in magnetic tunnel junctions is the tunnel magnetoresistance (TMR). This phenomenon appears as a change in the junction resistance when magnetic moments of external electrodes rotate from parallel alignment to non-collinear one (or to antiparallel alignment in a particular case). Such a rotation of magnetic moments may be induced, for instance, by an external magnetic field. The TMR effect may occur in planar junctions [3, 4, 5], mesoscopic double-barrier junctions [6, 7, 8, 9], granular systems [10, 11], and others. When the central part of a double-barrier junction is sufficiently small, the interplay of discrete charging by single electrons and spin dependence of tunnelling processes can lead to additional interesting features in the corresponding transport characteristics [6, 7, 8, 9].

Up to now, most of theoretical works on transport through quantum dots (QDs) coupled to ferromagnetic electrodes was limited to collinear, i.e., parallel and antiparallel magnetic configurations [12, 13, 14, 15, 16, 17, 18]. It is only very recently when transport in systems with non-collinear magnetizations was addressed [19, 20, 21, 22]. In particular, it has been shown that the diode-like features in transport characteristics of systems with one electrode being half-metallic are significantly reduced when magnetic moments of the electrodes become non-collinear [20]. However, this behavior was studied only in the sequential tunneling regime.

In recent papers [21, 22] spin precession in electron tunnelling through an interacting quantum dot was stud-

ied theoretically in the first order approximation with respect to the tunneling Hamiltonian. Such a precession takes place when magnetic moments of the leads are non-collinear, and occurs because an electron entering the dot in a tunnelling event is subject to an effective exchange field, which exerts a torque on the electron spin and makes the spin precesses by a certain angle before the electron leaves the dot. In the first order approximation, the spin precession is driven by the Coulomb interaction on the dot (described by the Hubbard correlation parameter U) and disappears when U tends to zero.

In this paper we extend the earlier descriptions [20, 21, 22] of electron tunneling through QD with non-collinear magnetizations by going beyond the first order approximation. In order to calculate the tunneling current and spin precession, we employ the non-equilibrium Green function technique and limit considerations to the Hartree-Fock approximation. Hence, besides the sequential tunneling also the contribution due to higher order tunneling processes is included in the description. Numerical results show, that spin precession also exist in the limit of $U = 0$. However, Coulomb correlations significantly enhance the precession. This, in turn, may lead to negative differential conductance in a certain bias voltage range. We predict that symmetry of the junction, barrier height, and spin polarization of magnetic leads may significantly influence spin dependent characteristics of the dot. In particular, it is shown that the diode-like behavior in asymmetrical junctions with one half-metallic electrode is partially suppressed in non-collinear configurations. However, the suppression is much less evident than that obtained within a simplified theory neglecting the exchange interactions between the dot and leads [20].

The paper is organized as follows. In Section II we

describe model of the system. Theoretical method is described in Section III, where the equation of motion method is used to derive nonequilibrium Green functions of the dot. Transport characteristics are calculated in Section IV, whereas relevant numerical results on tunnelling current, magnetoresistance, and spin precession are presented and discussed in Section V. Finally, summary and general conclusions are in Section VI.

II. MODEL

We consider a single-level QD coupled to two ferromagnetic metallic leads by tunnelling barriers. Magnetic moments in the external leads lie in a common plane and form an arbitrary angle φ . To describe electron spin we will use the local and global quantization axes. The local axes are determined by the local spin polarization in the leads. The global quantization axis (the axis z in our case) is assumed to coincide with the local one in the left electrode. Spin projection on the local quantization axes will be denoted as $\beta = +$ for majority electrons and $\beta = -$ for minority electrons, whereas projection on the global quantization axis will be denoted as $\sigma = \uparrow$ and $\sigma = \downarrow$. Axis y of the coordinate system is normal to the plane xz determined by the spin polarizations of the leads. Geometry of the device and the orientation of the coordinate system are shown schematically in Fig.1.

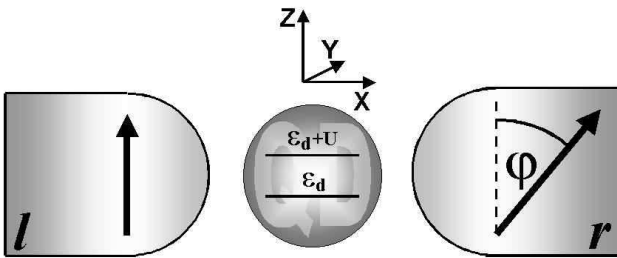


FIG. 1: Schematics of the system considered in this paper. The coordinate systems used to describe states of the dot is also shown.

The whole system can be described by Hamiltonian of the general form

$$H = H_l + H_r + H_d + H_t. \quad (1)$$

The term H_ν describes the left ($\nu = l$) and right ($\nu = r$) electrodes in the non-interacting quasi-particle approximation,

$$H_\nu = \sum_k \sum_{\beta=+,-} \varepsilon_{k\beta}^\nu a_{\nu k\beta}^+ a_{\nu k\beta}, \quad (2)$$

where $\varepsilon_{k\beta}^\nu$ is the single-electron energy in the ν -th electrode for the wavevector k and spin β , whereas $a_{\nu k\beta}^+$ and $a_{\nu k\beta}$ are the corresponding creation and annihilation operators. The term H_d in Eq.(1) describes QD,

$$H_d = \sum_\sigma \varepsilon_d c_\sigma^+ c_\sigma + U n_\uparrow n_\downarrow, \quad (3)$$

where $n_\sigma = c_\sigma^+ c_\sigma$ is the occupation operator, ε_d denotes the energy of the discrete level, U is the electron correlation parameter, whereas c_σ^+ and c_σ are the corresponding creation and annihilation operators for electrons with spin orientation $\sigma = \uparrow$ (\downarrow). Finally, the tunnelling term, H_t , in Eq.(1) takes the form

$$H_t = H_t^l + H_t^r, \quad (4)$$

where the first term describes tunnelling through the left barrier,

$$H_t^l = \sum_k (T_{k+}^l a_{lk+}^+ c_\uparrow + T_{k-}^l a_{lk-}^+ c_\downarrow) + \text{h.c.}, \quad (5)$$

whereas the second term corresponds to tunnelling through the right barrier,

$$H_t^r = \sum_k \{ [T_{k+}^r a_{rk+}^+ \cos(\varphi/2) - T_{k-}^r a_{rk-}^+ \sin(\varphi/2)] c_\uparrow \quad$$

$$+ [T_{k+}^r a_{rk-}^+ \cos(\varphi/2) + T_{k-}^r a_{rk+}^+ \sin(\varphi/2)] c_\downarrow \} + \text{h.c.}, \quad (6)$$

and h.c. stands for the hermitian conjugate terms. The tunneling terms H_t^l and H_t^r have different forms because the corresponding local and global axes are parallel for the left electrode and noncollinear for the right one.

III. GREEN FUNCTIONS OF THE DOT

To calculate electric current in nonequilibrium situations we will make use of the nonequilibrium Green function defined on the Keldysh contour [23]. The causal Green function of the dot is defined as $G_{\sigma\sigma'}(\epsilon) \equiv \langle \langle c_\sigma | c_{\sigma'}^+ \rangle \rangle_\epsilon$. Writing equation of motion for $\langle \langle c_\sigma | c_{\sigma'}^+ \rangle \rangle_\epsilon$, one arrives at

$$(\epsilon - \epsilon_d) \langle \langle c_\sigma | c_{\sigma'}^+ \rangle \rangle_\epsilon = \delta_{\sigma\sigma'} \quad + \sum_k [T_{k\beta}^{*l} \langle \langle a_{lk\beta} | c_{\sigma'}^+ \rangle \rangle_\epsilon + T_{k\beta}^{*r} \langle \langle a_{rk\beta} | c_{\sigma'}^+ \rangle \rangle_\epsilon \cos(\varphi/2) \quad - \beta T_{k-\beta}^{*r} \langle \langle a_{rk-\beta} | c_{\sigma'}^+ \rangle \rangle_\epsilon \sin(\varphi/2)] + U \langle \langle c_\sigma n_{-\sigma} | c_{\sigma'}^+ \rangle \rangle_\epsilon, \quad (7)$$

where $\beta = +$ for $\sigma = \uparrow$ and $\beta = -$ for $\sigma = \downarrow$. Applying equation of motion to the four new Green functions on the r.h.s. of Eq.(7), one finds

$$(\epsilon - \varepsilon_{k\beta}^l) \langle \langle a_{lk\beta} | c_{\sigma'}^+ \rangle \rangle_\epsilon = T_{k\beta}^l \langle \langle c_\sigma | c_{\sigma'}^+ \rangle \rangle_\epsilon, \quad (8)$$

$$(\epsilon - \varepsilon_{k\beta}^r) \langle \langle a_{rk\beta} | c_{\sigma'}^+ \rangle \rangle_\epsilon = T_{k\beta}^r \langle \langle c_\sigma | c_{\sigma'}^+ \rangle \rangle_\epsilon \cos(\varphi/2) \quad + \beta T_{k\beta}^r \langle \langle c_{-\sigma} | c_{\sigma'}^+ \rangle \rangle_\epsilon \sin(\varphi/2), \quad (9)$$

$$(\epsilon - \varepsilon_{k-\beta}^r) \langle \langle a_{rk-\beta} | c_{\sigma'}^+ \rangle \rangle_\epsilon = T_{k-\beta}^r \langle \langle c_{-\sigma} | c_{\sigma'}^+ \rangle \rangle_\epsilon \cos(\varphi/2) \quad - \beta T_{k-\beta}^r \langle \langle c_\sigma | c_{\sigma'}^+ \rangle \rangle_\epsilon \sin(\varphi/2), \quad (10)$$

$$\begin{aligned}
(\epsilon - \epsilon_d - U) \langle \langle c_\sigma n_{-\sigma} | c_{\sigma'}^+ \rangle \rangle_\epsilon &= \langle \{c_\sigma n_{-\sigma}, c_{\sigma'}^+ \} \rangle + \sum_k [T_{k\beta}^{*l} \langle \langle a_{lk\beta} | c_{\sigma'}^+ \rangle \rangle_\epsilon + T_{k\beta}^{*r} \langle \langle a_{rk\beta} n_{-\sigma} | c_{\sigma'}^+ \rangle \rangle_\epsilon \cos(\varphi/2) \\
&\quad - \beta T_{k-\beta}^{*r} \langle \langle a_{rk-\beta} n_{-\sigma} | c_{\sigma'}^+ \rangle \rangle_\epsilon \sin(\varphi/2) - T_{k-\beta}^l \langle \langle c_\sigma a_{lk-\beta}^+ c_{-\sigma} | c_{\sigma'}^+ \rangle \rangle_\epsilon - T_{k-\beta}^{*l} \langle \langle c_\sigma a_{lk-\beta} c_{-\sigma}^+ | c_{\sigma'}^+ \rangle \rangle_\epsilon \\
&\quad - T_{k-\beta}^r \langle \langle c_\sigma a_{rk-\beta}^+ c_{-\sigma} | c_{\sigma'}^+ \rangle \rangle_\epsilon \cos(\varphi/2) - \beta T_{k\beta}^r \langle \langle c_\sigma a_{rk\beta}^+ c_{-\sigma} | c_{\sigma'}^+ \rangle \rangle_\epsilon \sin(\varphi/2) \\
&\quad - T_{k-\beta}^{*r} \langle \langle c_\sigma a_{rk-\beta} c_{-\sigma}^+ | c_{\sigma'}^+ \rangle \rangle_\epsilon \cos(\varphi/2) - \beta T_{k\beta}^{*r} \langle \langle c_\sigma a_{rk\beta} c_{-\sigma}^+ | c_{\sigma'}^+ \rangle \rangle_\epsilon \sin(\varphi/2)]. \tag{11}
\end{aligned}$$

Now, the Hartree-Fock decoupling scheme is applied to the higher-order Green functions generated on the r.h.s. of eq. (11),

$$\langle \langle a_{\nu k \pm \beta} n_{-\sigma} | c_{\sigma'}^+ \rangle \rangle_\epsilon \rightarrow \langle n_{-\sigma} \rangle \langle \langle a_{\nu k \pm \beta} | c_{\sigma'}^+ \rangle \rangle_\epsilon, \tag{12}$$

$$\langle \langle c_\sigma a_{\nu k \pm \beta} c_{-\sigma}^+ | c_{\sigma'}^+ \rangle \rangle \rightarrow \langle c_{-\sigma}^+ c_\sigma \rangle \langle \langle a_{\nu k \pm \beta} | c_{\sigma'}^+ \rangle \rangle, \tag{13}$$

$$\langle \langle c_\sigma a_{\nu k \pm \beta}^+ c_{-\sigma} | c_{\sigma'}^+ \rangle \rangle \simeq 0, \tag{14}$$

which closes the set of equations (7)-(11) and allows to find solution for the causal Green functions $G_{\sigma\sigma'}(\epsilon)$. Here, $\langle \dots \rangle$ means the quantum statistical average value of the appropriate operator.

The solution may be written in the compact form of the matrix Dyson equation:

$$\mathbf{G}(\epsilon) = [\mathbf{1} - \mathbf{g}(\epsilon) \mathbf{\Sigma}(\epsilon)]^{-1} \mathbf{g}(\epsilon), \tag{15}$$

where

$$\mathbf{G}(\epsilon) = \begin{pmatrix} G_{\uparrow\uparrow}(\epsilon) & G_{\uparrow\downarrow}(\epsilon) \\ G_{\downarrow\uparrow}(\epsilon) & G_{\downarrow\downarrow}(\epsilon) \end{pmatrix}, \tag{16}$$

and $\mathbf{g}(\epsilon)$ denotes the corresponding Green functions in the matrix form of the uncoupled dot, with the matrix elements

$$g_{\sigma\sigma}(\epsilon) = \frac{\epsilon - \epsilon_d - U(1 - \langle n_{-\sigma} \rangle)}{(\epsilon - \epsilon_d)(\epsilon - \epsilon_d - U)}, \tag{17}$$

$$g_{\sigma-\sigma}(\epsilon) = -\frac{U \langle n_{-\sigma\sigma} \rangle}{(\epsilon - \epsilon_d)(\epsilon - \epsilon_d - U)}, \tag{18}$$

with $\langle n_{-\sigma\sigma} \rangle = \langle c_{-\sigma}^+ c_\sigma \rangle$.

Finally, the self-energy $\mathbf{\Sigma}(\epsilon)$ is given by

$$\mathbf{\Sigma}(\epsilon) = \begin{pmatrix} \Sigma_{0+}(\epsilon) & \Sigma_1(\epsilon) \\ \Sigma_1(\epsilon) & \Sigma_{0-}(\epsilon) \end{pmatrix}, \tag{19}$$

with

$$\begin{aligned}
\Sigma_{0\pm}(\epsilon) &= \sum_k \frac{|T_{k\pm}^l|^2}{\epsilon - \varepsilon_{k\pm}^l} \\
&+ \sum_k \left(\frac{|T_{k\pm}^r|^2}{\epsilon - \varepsilon_{k\pm}^r} \cos^2(\varphi/2) + \frac{|T_{k\mp}^r|^2}{\epsilon - \varepsilon_{k\mp}^r} \sin^2(\varphi/2) \right) \tag{20}
\end{aligned}$$

and

$$\Sigma_1(\epsilon) = \frac{1}{2} \sum_k \left(\frac{|T_{k+}^r|^2}{\epsilon - \varepsilon_{k+}^r} - \frac{|T_{k-}^r|^2}{\epsilon - \varepsilon_{k-}^r} \right) \sin \varphi. \tag{21}$$

Having found the causal Green functions one can calculate the retarded (advanced) Green functions $G_{\sigma\sigma'}^{R(A)}(\epsilon) = G_{\sigma\sigma'}(\epsilon \pm i\eta)$,

$$G_{\uparrow\uparrow}^R(\epsilon) = [g_{\uparrow\uparrow}^R(\epsilon) - A \Sigma_{0-}^R(\epsilon)]/B, \tag{22}$$

$$G_{\uparrow\downarrow}^R(\epsilon) = [g_{\uparrow\downarrow}^R(\epsilon) + A \Sigma_1^R(\epsilon)]/B, \tag{23}$$

$$G_{\downarrow\uparrow}^R(\epsilon) = [g_{\downarrow\uparrow}^R(\epsilon) + A \Sigma_1^R(\epsilon)]/B, \tag{24}$$

$$G_{\downarrow\downarrow}^R(\epsilon) = [g_{\downarrow\downarrow}^R(\epsilon) - A \Sigma_{0+}^R(\epsilon)]/B, \tag{25}$$

where

$$A = g_{\uparrow\uparrow}^R(\epsilon) g_{\downarrow\downarrow}^R(\epsilon) - g_{\uparrow\downarrow}^R(\epsilon) g_{\downarrow\uparrow}^R(\epsilon), \tag{26}$$

$$\begin{aligned}
B &= 1 - \{g_{\uparrow\uparrow}^R(\epsilon) \Sigma_{0+}^R(\epsilon) + g_{\downarrow\downarrow}^R(\epsilon) \Sigma_{0-}^R(\epsilon) + [g_{\uparrow\downarrow}^R(\epsilon) \\
&\quad + g_{\downarrow\uparrow}^R(\epsilon)] \Sigma_1^R(\epsilon) + [g_{\uparrow\uparrow}^R(\epsilon) g_{\downarrow\downarrow}^R(\epsilon) - g_{\uparrow\downarrow}^R(\epsilon) g_{\downarrow\uparrow}^R(\epsilon)] \\
&\quad \times \{\Sigma_{0+}^R(\epsilon) \Sigma_{0-}^R(\epsilon) - [\Sigma_1^R(\epsilon)]^2\}. \tag{27}
\end{aligned}$$

The retarded self energies $\Sigma_{0\pm}^R(\epsilon)$ and $\Sigma_1^R(\epsilon)$ are given by the formulae

$$\begin{aligned}
\Sigma_{0\pm}^R(\epsilon) &= -\frac{1}{2} \Gamma_{\pm}^l(\epsilon) \left[\frac{1}{\pi} \ln \left(\frac{D + eV_l - \epsilon}{D - eV_l + \epsilon} \right) + i \right] \\
&\quad - \frac{1}{2} \left[\Gamma_{\pm}^r(\epsilon) \cos^2(\varphi/2) + \Gamma_{\mp}^r(\epsilon) \sin^2(\varphi/2) \right] \\
&\quad \times \left[\frac{1}{\pi} \ln \left(\frac{D + eV_r - \epsilon}{D - eV_r + \epsilon} \right) + i \right] \tag{28}
\end{aligned}$$

and

$$\begin{aligned}
\Sigma_1^R(\epsilon) &= -\frac{1}{4} [\Gamma_+^r(\epsilon) - \Gamma_-^r(\epsilon)] \sin \varphi \\
&\quad \times \left[\frac{1}{\pi} \ln \left(\frac{D + eV_r - \epsilon}{D - eV_r + \epsilon} \right) + i \right], \tag{29}
\end{aligned}$$

where

$$\Gamma_{\pm}^{\nu}(\epsilon) = 2\pi \sum_k |T_{k\pm}^{\nu}|^2 \delta(\epsilon - \epsilon_{k\pm}^{\nu}) \quad (30)$$

for $\nu = l, r$. It has been assumed that the lower and upper edges of the electron band at zero bias are at $-D$ and D , respectively.

In the following we assume

$$\Gamma_{\pm}^l(\epsilon) = \Gamma_{\pm}^r = \Gamma_0(1 \pm p_l) \quad (31)$$

and

$$\Gamma_{\pm}^r(\epsilon) = \Gamma_{\pm}^l = \alpha \Gamma_0(1 \pm p_r) \quad (32)$$

when ϵ is within the electron band and zero otherwise. The parameters p_l and p_r describe the spin asymmetry of the coupling to the left and right electrodes, respectively, Γ_0 is a constant, and the parameter α takes into account asymmetry between coupling of the dot to the left and right electrodes.

Since the self-energies given explicitly by Eqs. (28) and (29) are independent of U in the Hartree-Fock approximation, one can calculate the correlation Green function from the Keldysh equation,

$$\mathbf{G}^<(\epsilon) = \mathbf{G}^R(\epsilon) \Sigma^<(\epsilon) \mathbf{G}^A(\epsilon), \quad (33)$$

where

$$\Sigma^<(\epsilon) = - \sum_{\nu} [\Sigma_{\nu}^R(\epsilon) - \Sigma_{\nu}^A(\epsilon)] f_{\nu}(\epsilon), \quad (34)$$

and $f_{\nu}(\epsilon)$ is the Fermi-Dirac distribution function for the ν -th electrode, $f_{\nu}(\epsilon) = 1/\{1 + \exp[(\epsilon - \mu_{\nu})/k_B T]\}$, with the electrochemical potentials $\mu_l = eV_l = eV/2$ and $\mu_r = eV_r = -eV/2$. The energy is measured from the Fermi level of the leads in equilibrium.

The average values of the occupation numbers $\langle n_{\sigma} \rangle = \langle c_{\sigma}^+ c_{\sigma} \rangle$ and $\langle n_{\sigma-\sigma} \rangle = \langle c_{\sigma}^+ c_{-\sigma} \rangle$ (which enter the expressions for Green functions) have to be calculated self-consistently by using the formulae

$$\langle n_{\sigma} \rangle = \text{Im} \int_{-\infty}^{+\infty} \frac{d\epsilon}{2\pi} G_{\sigma\sigma}^<(\epsilon) \quad (35)$$

and

$$\langle n_{\sigma-\sigma} \rangle = -i \int_{-\infty}^{+\infty} \frac{d\epsilon}{2\pi} G_{-\sigma\sigma}^<(\epsilon). \quad (36)$$

IV. TRANSPORT CHARACTERISTICS

Having found the Green functions, one can calculate electric current, spin accumulation, and spin precession on the dot. To do this we calculate the average values of all the three spin components, which are related to the diagonal and off-diagonal occupation numbers (Eqs (35) and (36)). The corresponding relations may be written as (spin components are measured in the units of \hbar),

$$\langle S_z \rangle = (n_{\uparrow} - n_{\downarrow})/2, \quad (37)$$

$$\langle S_y \rangle = \text{Im}(n_{\uparrow\downarrow}), \quad (38)$$

$$\langle S_x \rangle = \text{Re}(n_{\uparrow\downarrow}), \quad (39)$$

where n_{\uparrow} , n_{\downarrow} , and $n_{\uparrow\downarrow}$ are calculated self-consistently, as described above.

In turn, electric current flowing from the ν -th lead to the dot is given by the formula [24]

$$J_{\nu} = \frac{ie}{\hbar} \int_{-\infty}^{+\infty} \frac{d\epsilon}{2\pi} \text{Tr} \left\{ \Gamma_{\nu} (\mathbf{G}^<(\epsilon) + f_{\nu}(\epsilon) [\mathbf{G}^R(\epsilon) - \mathbf{G}^A(\epsilon)]) \right\}, \quad (40)$$

with

$$\Gamma_l = \Gamma_0 \begin{pmatrix} 1 + p_l & 0 \\ 0 & 1 - p_l \end{pmatrix} \quad (41)$$

and

$$\Gamma_r = \Gamma_0 \alpha \begin{pmatrix} 1 + p_r \cos \varphi & p_r \sin \varphi \\ p_r \sin \varphi & 1 - p_r \cos \varphi \end{pmatrix}. \quad (42)$$

Thus, taking into account Eqs (22)-(34), together with Eqs (40)-(42), one obtains the final symmetrized expression for electric current, $J = (1/2)(J_l - J_r)$, in the form

$$J = \frac{e\alpha\Gamma_0^2}{4\pi\hbar} \int_{-\infty}^{+\infty} d\epsilon [f_l(\epsilon) - f_r(\epsilon)] j(\epsilon), \quad (43)$$

where

$$\begin{aligned} j(\epsilon) = & 2(1 + p_l)(1 + p_r \cos \varphi) G_{\uparrow\uparrow}^R(\epsilon) G_{\uparrow\uparrow}^{R*}(\epsilon) + 2(1 - p_l)(1 - p_r \cos \varphi) G_{\downarrow\downarrow}^R(\epsilon) G_{\downarrow\downarrow}^{R*}(\epsilon) \\ & + [(1 + p_l)(1 - p_r \cos \varphi) + (1 - p_l)(1 + p_r \cos \varphi)] [G_{\uparrow\downarrow}^R(\epsilon) G_{\uparrow\downarrow}^{R*}(\epsilon) + G_{\downarrow\uparrow}^R(\epsilon) G_{\downarrow\uparrow}^{R*}(\epsilon)] \\ & + (1 + p_l)p_r \sin \varphi \{G_{\uparrow\uparrow}^R(\epsilon) [G_{\uparrow\downarrow}^{R*}(\epsilon) + G_{\downarrow\uparrow}^{R*}(\epsilon)] + G_{\uparrow\downarrow}^{R*}(\epsilon) [G_{\uparrow\uparrow}^R(\epsilon) + G_{\downarrow\uparrow}^R(\epsilon)]\} \\ & + (1 - p_l)p_r \sin \varphi \{G_{\downarrow\downarrow}^R(\epsilon) [G_{\uparrow\downarrow}^{R*}(\epsilon) + G_{\downarrow\uparrow}^{R*}(\epsilon)] + G_{\uparrow\downarrow}^{R*}(\epsilon) [G_{\downarrow\downarrow}^R(\epsilon) + G_{\downarrow\uparrow}^R(\epsilon)]\}. \end{aligned} \quad (44)$$

The current formula derived above can be applied to any magnetic configuration of the system, and thus can be used to determine TMR. Generally, TMR is described quantitatively by the ratio

$$TMR = \frac{R(\varphi) - R(\varphi = 0)}{R(\varphi = 0)} = \frac{J(\varphi = 0) - J(\varphi)}{J(\varphi)}, \quad (45)$$

where $J(\varphi)$ is the electric current flowing through the system when the angle between spin polarizations of the leads is φ , and $R(\varphi)$ is the corresponding electrical resistance.

V. NUMERICAL RESULTS

A. Symmetrical junctions

In a symmetrical case both barriers are identical, $\alpha = 1$, and the electrodes are made of the same ferromagnetic material, $p_l = p_r$. Consider first electronic transport in a symmetrical junction with fully polarized (half-metallic) external electrodes, $p_l = p_r = 1$, and with the dot level above the Fermi level of the electrodes at equilibrium, $\varepsilon_d > 0$.

Bias dependence of electric current and the corresponding differential conductance are shown in Fig.2(a) and Fig.2(b) for selected values of the angle φ . The current-voltage curve for parallel configuration ($\varphi = 0$) reveals typical step-like characteristics. Below the first (lower) threshold voltage the dot is empty and thus sequential contribution to electric current is exponentially suppressed. The first step in the current occurs at the bias, where the discrete level ε_d crosses the Fermi level of the source electrode (the dot can be occupied by a single electron), whereas the step at a higher voltage (higher threshold) corresponds to the case when $\varepsilon_d + U$ crosses this Fermi level (the dot may be doubly occupied).

In non-collinear configurations a monotonous suppression of the tunneling current with increasing φ takes place in the whole bias voltage range, and the current disappears for $\varphi = \pi$. This is a typical (perfect) spin-valve effect. Suppression of electric current is due to an electron residing on the dot, whose spin orientation prevents it from tunneling to the drain lead. In the extreme case of antiparallel configuration, $\varphi = \pi$, the electron that has tunneled to the dot from the fully polarized source electrode blocks transport through the junction since it cannot tunnel further to the oppositely polarized drain lead. This scenario holds as long as spin-flip relaxation processes are absent.

The steps in current-voltage characteristics give rise to the narrow peaks in differential conductance displayed in Fig.2(b), which occur at the lower and higher threshold voltages. Apart from this, dependence of electric current on magnetic configuration of the system leads to the TMR effect, defined quantitatively by Eq.(45), and is shown in Fig.2(c). The effect increases with increas-

ing angle φ and tends to infinity when $\varphi \rightarrow \pi$ (therefore there is no curve in Fig.2(c) for $\varphi = \pi$).

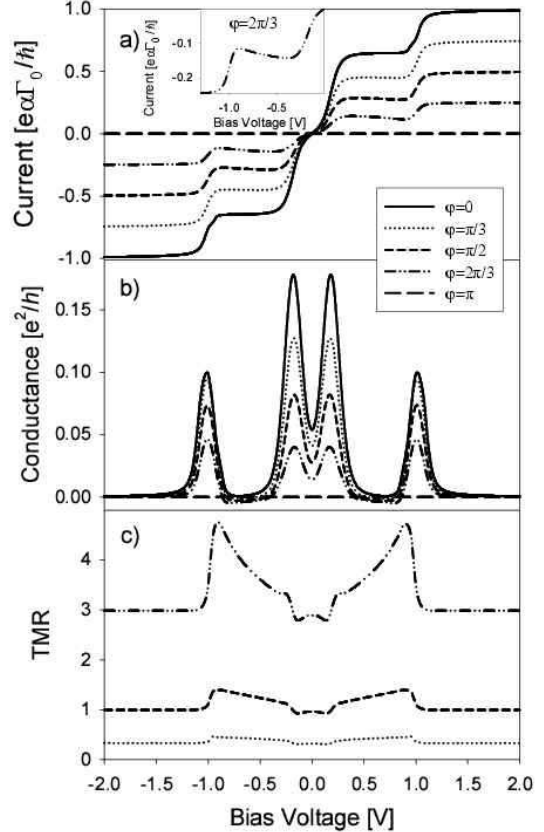


FIG. 2: Bias dependence of electric current (a), differential conductance (b), and tunnel magnetoresistance (c), calculated for indicated values of the angle φ . The inset in (a) shows electric current between the lower and higher threshold voltages for $\varphi = 2\pi/3$. The parameters assumed for numerical calculations are: $\varepsilon_d = 0.1$ eV, $U = 0.4$ eV, $\Gamma_0 = 0.01$ eV, $p_l = p_r = 1$, $\alpha = 1$ and $T = 100$ K.

An interesting feature of the current-voltage characteristics is the negative differential conductance, which may occur in non-collinear configurations between the lower and higher threshold voltages (between the corresponding two peaks in the differential conductance). The negative differential conductance corresponds to some enhancement in TMR, as can be seen in Fig.2(c). The enhancement is particularly significant for rather large values of the angle φ (smaller than π). Physical origin of this feature becomes clear, when taking into account bias dependence of the average spin on the dot in nonequilibrium situation (spin accumulated on the dot). As shown in Fig.3(a), the absolute value of the average $\langle S_z \rangle$ increases with increasing φ and almost vanishes in the parallel configuration. In turn, the average value of the x -component, $\langle S_x \rangle$, vanishes for both parallel and antiparallel alignments and is nonzero for canted configurations.

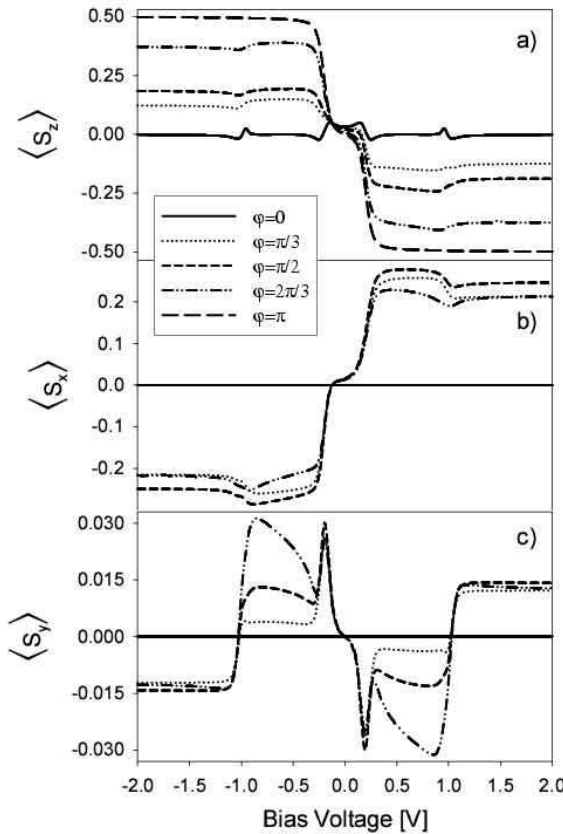


FIG. 3: Bias dependence of the average spin components; $\langle S_z \rangle$ (a), $\langle S_x \rangle$ (b) and $\langle S_y \rangle$ (c) for indicated values of the angle φ . The other parameters are as in Fig.2.

tions, as shown in Fig.3(b). Similarly, the average value of $\langle S_y \rangle$ also vanishes in the collinear configurations and is nonzero in the noncollinear ones. One should point here, that neither initial spin state in the source electrode, nor the final state in the drain electrode have nonvanishing y -component (perpendicular to the plane determined by spin polarizations of the two leads). What is then the reason of nonvanishing $\langle S_y \rangle$? This can be accounted for by taking into account the fact, that an electron residing on the dot experiences a certain exchange field resulting from coupling between the dot and leads, which effectively acts as a local magnetic field [22]. Strength of this molecular field and its orientation with respect to the global quantization axis depend on the applied bias voltage and on the angle between the magnetic moments of the leads. Thus, if an electron that has tunneled from the source lead resides sufficiently long time on the dot level, its spin experiences a torque due to the exchange interaction, which results in precession of the average spin around the molecular field, and consequently in a nonzero average value of the transverse component $\langle S_y \rangle$. As shown in Fig.3(c), this precession-induced com-

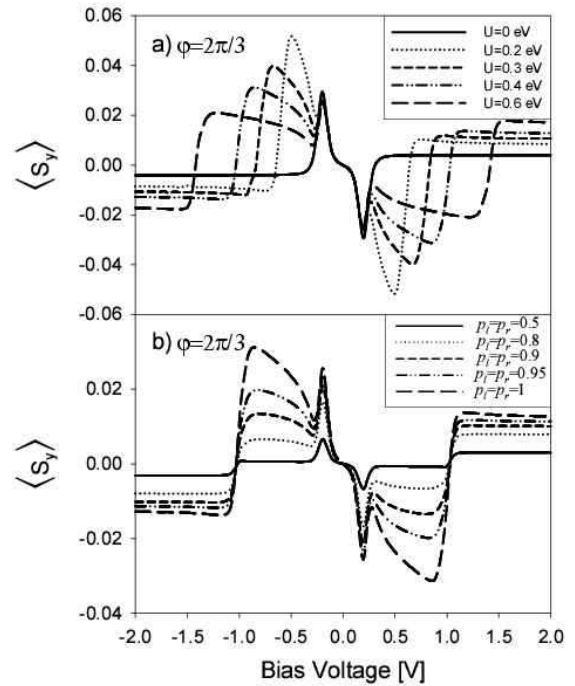


FIG. 4: Bias dependence of the average spin component $\langle S_y \rangle$ for $\varphi = 2\pi/3$ and for indicated values of the Coulomb correlation parameter U (a) and the lead polarization (b). The other parameters are as in Fig.2.

ponent is significant in non-collinear cases (see the case of $\varphi = 2\pi/3$) and in the voltage range between the two threshold voltages. Just this enhanced precession is associated with a decrease in electric current, which leads to negative differential conductance.

As follows from the above discussion, the magnitude of $\langle S_y \rangle$ is a measure of the spin precession induced by the effective exchange field. In Fig.4(a) we show $\langle S_y \rangle$ for different values of the Coulomb correlation parameter U . The curve for $U = 0$ indicates that spin precession in noncollinear configurations takes place also when there is no Coulomb interaction between electrons on the dot. However, as follows from Fig.4(a), the presence of such an interaction enhances the spin precession and also extends the voltage range where the precession is significant.

The spin precession also depends on the spin polarization of external electrodes. This is shown in Fig.4(b), where the y -component of the average spin accumulated on the dot is shown for several values of the parameters p_l and p_r . This figure clearly shows that the spin precession decreases when spin polarization of the leads

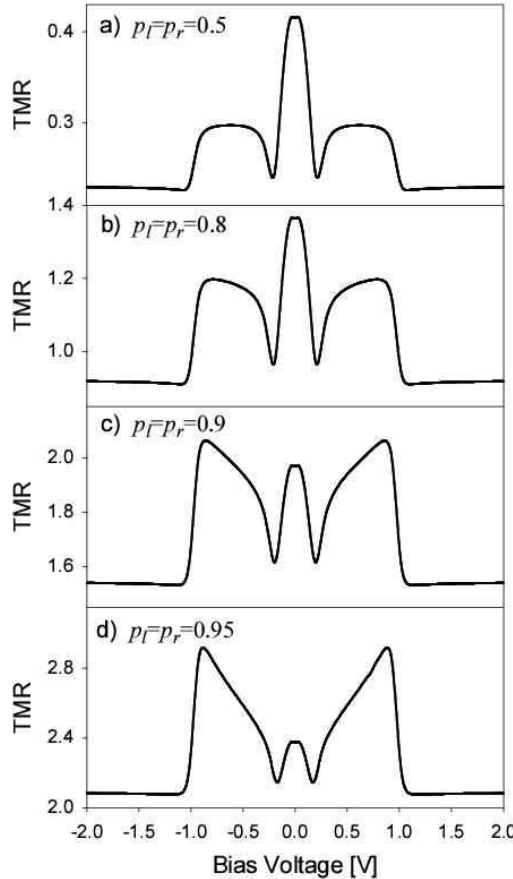


FIG. 5: Bias dependence of the tunnel magnetoresistance in symmetrical junctions for indicated values of the lead polarization. The curves are plotted for the non-collinear configuration, $\varphi = 2\pi/3$. The other parameters are as in Fig.2.

becomes smaller. This is reasonable since lower spin polarization creates smaller exchange field.

When the spin polarization rate of the leads becomes smaller than 1, electric current can flow also in the antiparallel configuration, contrary to the case shown in Fig.2 for $p_l = p_r = 1$. Consequently, the TMR effect also becomes smaller and remains finite for $\varphi = \pi$. In Fig.5 we show the TMR effect for different polarizations of the external electrodes, and for a particular noncollinear configuration ($\varphi = 2\pi/3$). The curves are symmetrical with respect to the bias reversal. The central peak corresponds to an enhanced magnetoresistance in the current blockade regime. Such an enhancement of TMR in the blockade regime, where sequential tunneling is suppressed, was also observed earlier for collinear configurations [14]. Although the sequential current is exponentially suppressed in the blockade regime, the electrons still can flow due to higher order processes (like cotunneling). The other two broad maxima placed symmetrically on both sides of the central peak, occur between the two (lower and higher)

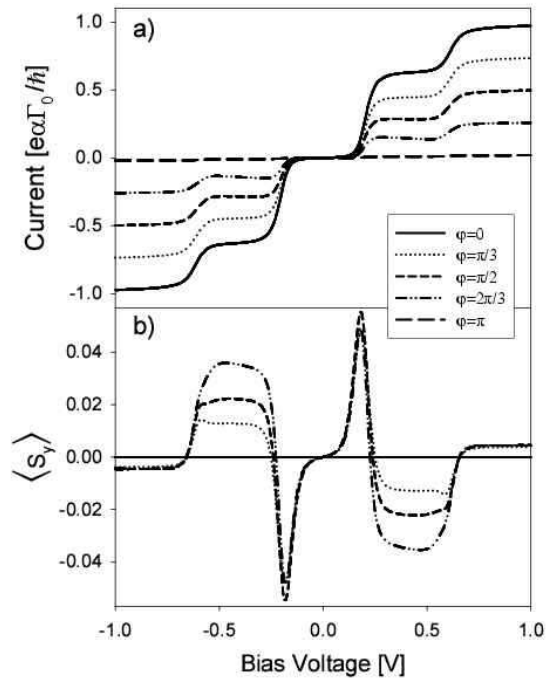


FIG. 6: Bias dependence of electric current (a), and the average value of the y component of the dot spin (b), calculated for indicated values of the angle φ and $\varepsilon_d = -0.1$ eV. The other parameters are as in Fig.2.

threshold voltages. The following features of these two maxima are interesting to note. First, for small values of the polarization parameters, the central maximum is larger than the others. The situation changes with increasing polarization factors, and now the central peak becomes smaller for high spin polarizations of the leads. Second, the two maxima become strongly asymmetric for large values of the spin polarization factors, as clearly visible in Fig.5. To account for this behavior one should take into account bias dependence of $\langle S_y \rangle$ from Fig.4(b), which shows clearly the correlations between the spin precession and height and shape of the TMR peaks with increasing polarization.

In the situation studied above the dot level was empty at equilibrium. Qualitatively similar behavior of electric current, magnetoresistance, and average spin on the dot, has been found for the situation when the dot level is below the Fermi level, and the dot is occupied by a single electron at equilibrium. Exemplary current-voltage characteristics are shown in Fig.6(a), and the corresponding

y -components of the average spin on the dot are shown

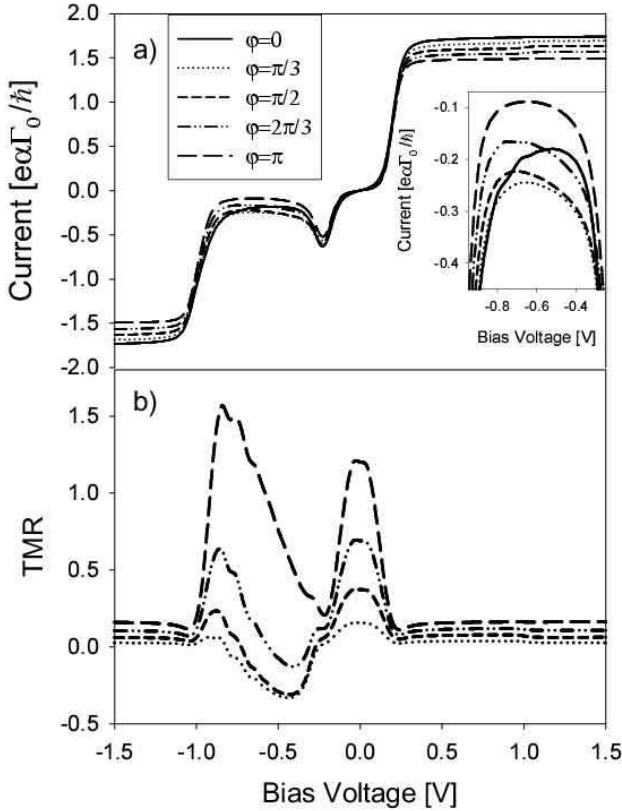


FIG. 7: Bias dependence of electric current (a) and magnetoresistance (b), calculated for indicated values of the angle φ . The inset in (a) shows current between the threshold voltages for negative bias. The parameters assumed for numerical calculations are: $\varepsilon_d = 0.1$ eV, $U = 0.4$ eV, $\Gamma_0 = 0.01$ eV, $p_l = 0.4$, $p_r = 1$, $\alpha = 0.1$ and $T = 100$ K.

in Fig.6(b). The current-voltage curves display similar features as the curves shown in Fig.2(a), with characteristic negative differential conductance between the threshold voltages for noncollinear configurations. The main difference in the bias dependence of $\langle S_y \rangle$ is a reversed sign of the peaks at the lower threshold voltage in comparison to that in Fig.3(c).

B. Asymmetrical junctions

Now the dot is separated from both electrodes by non-equivalent barriers, $\alpha \neq 1$, and the electrodes are made of different ferromagnetic materials, $p_l \neq p_r$. For numerical calculations we assume $p_l=0.4$, $p_r=1$, and $\alpha = 0.1$. More specifically, it is assumed that the right electrode is made of a half-metallic material with electrons being totally spin-polarized at the Fermi level, whereas the factor $\alpha = 0.1$ indicates that on average electrons can

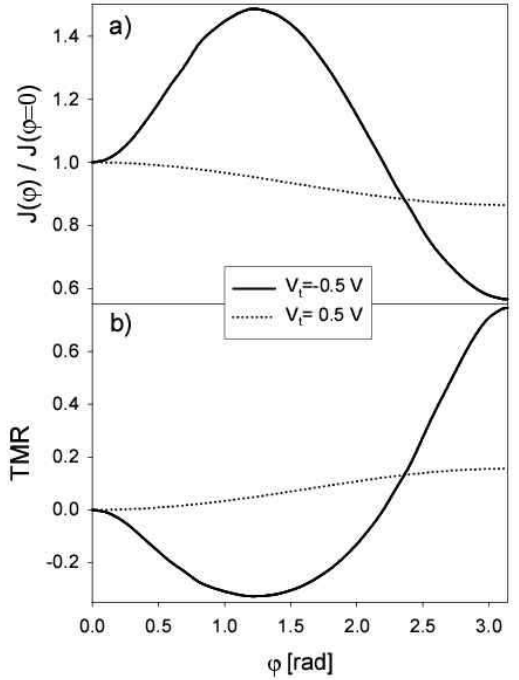


FIG. 8: Angular variation of electric current (a) and TMR (b) for indicated values of the bias voltage. The other parameters are as in Fig.7.

tunnel much easier to (from) the left electrode than to (from) the right one. This asymmetry between the left and right electrodes and barriers gives rise to asymmetrical transport characteristics of the junction with respect to the bias reversal. The asymmetry is clearly visible in current-voltage characteristics and bias dependence of TMR, shown in Fig.7(a) and Fig.7(b), respectively. For positive bias (the right lead is the source electrode), the current and TMR curves are rather uniform above the first threshold voltage. The current flows there for arbitrary value of the angle φ and thus TMR is significantly suppressed. The situation changes diametrically when the electric current flows in the opposite direction, i.e. when electrons tunnel through the dot from the left electrode to the right (half-metallic) one. Below the first threshold voltage sequential tunneling is exponentially suppressed and only the higher-order tunneling processes are possible. When the energy level ε_d enters the tunneling window, electric current starts to flow through the junction but this takes place only in a small voltage range in the vicinity of the first threshold voltage, where

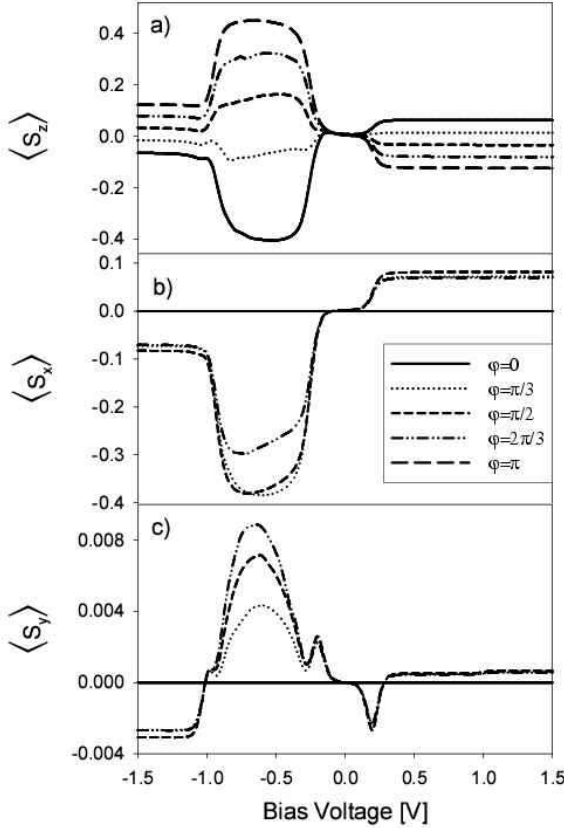


FIG. 9: Bias dependence of the average spin components; $\langle S_z \rangle$ (a), $\langle S_x \rangle$ (b) and $\langle S_y \rangle$ (c) for indicated values of the angle φ . The other parameters are as in Fig.6.

the characteristic resonant bump is observed. Above the bump, the current is suppressed by an electron residing on the dot. When $\varepsilon_d + U$ crosses the Fermi level of the source lead, the current increases again and finally saturates at a certain level. For positive bias, $V > 0$, the curves in Fig.7(a) and Fig.7(b) for different values of the angle φ reflect a monotonous angular variation of the current and TMR, shown also explicitly in Fig.8 for a particular value of the bias voltage. For negative bias one observes a more complex and interesting behavior of the transport characteristics. First, the above mentioned suppression of electric current between the two steps is now less pronounced, and the corresponding angular variation of electric current and TMR is non-monotonous, as shown explicitly in Fig.8 by the relevant curve. When the negative bias voltage surpasses the second threshold, the monotonous variation of electric current and TMR is restored. It is also interesting to note, that the TMR effect is enhanced in the voltage regions, where electric current is suppressed. This is the region below the first threshold voltage, and for negative bias also the region

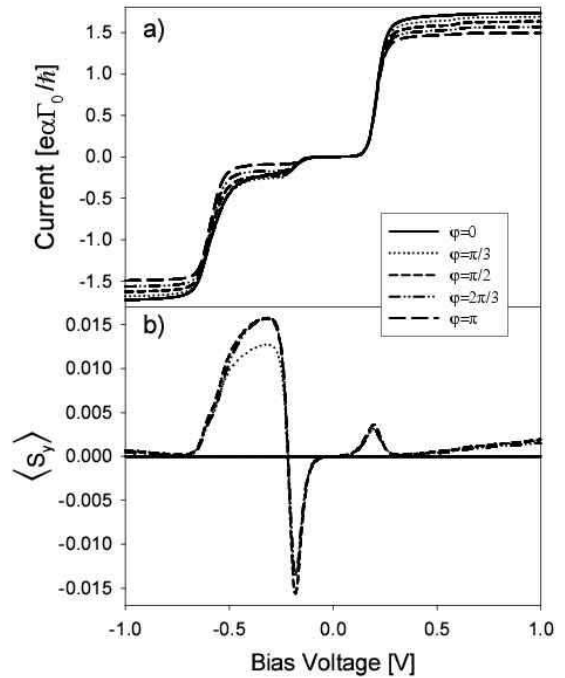


FIG. 10: Bias dependence of electric current (a), and the average value of the y component of the dot spin (b), calculated for indicated values of the angle φ and $\varepsilon_d = -0.1$ eV. The other parameters are as in Fig.7.

between the two threshold voltages. The latter one is particularly interesting as the TMR may change there sign from positive to negative (see Fig.7(b) and Fig.8(b)).

Suppression of electric current by an electron of a given spin orientation localized on the dot can be accounted for by analyzing spin accumulated on the dot when a steady state current flows through the system. This is illustrated in Fig.9(a-c), where the part (c) shows the component induced by spin precession. The spin precession is particularly enhanced for negative bias between the two thresholds - exactly where electric current is suppressed. The enhancement is a consequence of relatively long time that electrons spend on the dot.

The situation is different for the dot level lying under the Fermi level, i.e., when the dot is already occupied by one electron in equilibrium situation. The corresponding numerical results are shown in Fig.10, where part (a) shows the current-voltage characteristics, and part (b) the average value of the perpendicular y -component of the average spin accumulated on the dot. The transport characteristics for collinear configurations were already

accounted for in earlier publications [13], and their most interesting feature is the pronounced asymmetry with respect to the bias reversal (diode-like behavior). For noncollinear configurations transport characteristics have new features, which are qualitatively similar to those found in the case of empty dot at equilibrium, like for instance nonmonotonous angular variation of electric current and TMR.

VI. SUMMARY AND CONCLUSIONS

Using the non-equilibrium Green function approach we have calculated electric current, average value of electron spin accumulated on the dot, and tunnel magnetoresistance due to rotation of the magnetic moments of external electrodes. It has been shown that the average spin precesses by a certain angle around an effective exchange field arising from the interaction between the dot and electrodes. This precession leads to a nonzero value of

$\langle S_y \rangle$, i.e., of the component normal to the plane determined by magnetic moments of both electrodes.

It has been also shown that the spin precession is enhanced by Coulomb correlations and strong spin polarization of the leads. The spin precession is shown to exist also in the limit of vanishing Coulomb correlations on the dot. Moreover, the interplay of Coulomb correlations and effective exchange field may lead to a negative differential conductance in the voltage range between the two threshold voltages. It has been also shown, that the diode-like features of the system are partially suppressed when magnetic moments of the electrodes become non-collinear.

Acknowledgments

The work was supported by the State Committee for Scientific Research through the Research Project PBZ/KBN/044/P03/2001 and 4 T11F 014 24.

[1] G.A. Prinz, *J. Magn. Magn. Materials* **200**, 57 (1999).
[2] J.M. Daughton, *J. Magn. Magn. Materials* **192**, 334 (1999).
[3] J.S. Moodera, L.R. Kinder, T.M. Wong and R. Meservey, *Phys. Rev. Lett.* **74**, 3273 (1995).
[4] S.S.P. Parkin, K.P. Roche, M.G. Samant, P.M. Rice, R.B. Beyers, R.E. Scheuerlein, E.J. O'Sullivan, S.L. Brown, J. Guchigano, D.W. Abraham, Yu Lu, M. Rooks, P.L. Trouilloud, R.A. Wanner, and W.J. Gallagher, *J. Appl. Phys.* **88**, 5828 (1999).
[5] X. Zhang, B.S. Li, G. Sun, and F.C. Pu, *Phys. Rev. B* **56**, 5484 (1997); M. Wilczyński and J. Barnaś, *J. Magn. Magn. Mater.* **221**, 373 (2000).
[6] J. Barnaś and A. Fert, *Phys. Rev. Lett.* **80**, 2058 (1998); *Europhys. Lett.* **44**, 85 (1998).
[7] J. Barnaś and A. Fert, *J. Magn. Magn. Mater.* **192**, L 351 (1999).
[8] S. Takahashi and S. Maekawa, *Phys. Rev. Lett.* **80**, 1758 (1998).
[9] A. Brataas, Yu.V. Nazarov, J. Inoue, and G.E.W. Bauer, *European Phys. Journ. B* **9**, 421 (1999); X.H. Wang and A. Brataas, *Phys. Rev. Lett.* **83**, 5138 (1999).
[10] H. Imamura, J. Chiba, S. Mitani, K. Takanashi, S. Takahashi, S. Maekawa, and H. Fujimori, *Phys. Rev. B* **61**, 46 (2000).
[11] K. Yakushiji, S. Mitani, K. Takanashi, S. Takahashi, S. Maekawa, H. Imamura, and H. Fujimori, *Appl. Phys. Lett.* **78**, 515 (2001).
[12] B.R. Bulka, *Phys. Rev. B* **62**, 3186 (2000).
[13] W. Rudziński and J. Barnaś, *Phys. Rev. B* **69**, 085318 (2001).
[14] R.Świrkowicz, J. Barnaś, and M. Wilczyński, *J. Phys.: Condens. Matter* **14**, 2011 (2002).
[15] J. Fransson, O. Eriksson, and I. Sandalov, *Phys. Rev. Lett.* **88**, 226601 (2002).
[16] B.R. Bulka and S. Lipiński, *Phys. Rev. B* **67**, 024404 (2003).
[17] J. Martinek, Y. Utsumi, H. Imamura, J. Barnaś, S. Maekawa, J. König, G. Schön, *Phys. Rev. Lett.* **91**, 127203 (2003).
[18] R. Lopez and D. Sanchez, *Phys. Rev. Lett.* **90**, 116602 (2003).
[19] N. Sergueev, Q.F. Sun, H. Guo, B. G. Wang, and J. Wang, *Phys. Rev. B* **65**, 165303 (2002).
[20] J. Barnaś, R. V. Dugaev, S. Krompiewski, J. Martinek, W. Rudziński, Świrkowicz, I. Weymann, M. Wilczyński, *phys. status solidi (b)* **236**, 246 (2003).
[21] J. König and J. Martinek, *Phys. Rev. Lett.* (2003).
[22] M. Braun, J. König and J. Martinek, *cond-mat/0404455* v1 (2004).
[23] H. Haug, and A.-P. Jauho, *Quantum Kinetics in Transport and Optics of Semiconductors*, Springer Verlag, Berlin 1996, p.170.
[24] A.-P. Jauho, N.S. Wingreen, and Y. Meir, *Phys. Rev. B* **50**, 5528 (1994).
[25] I. Weymann, J. Martinek, J. König, J. Barnaś, and G. Schön, to be published.